

Toward General Digraph Contrastive Learning: A Dual Spatial Perspective

Daohan Su[†], Yang Zhang[†], Xunkai Li[†], Rong-Hua Li[†], Guoren Wang[†]

[†] Beijing Institute of Technology, Beijing, China

dhsu@bit.edu.cn, yangzhang.john@gmail.com,

cs.xunkai.li@gmail.com, lironghuabit@126.com, wanggrbit@gmail.com

Abstract—Graph Contrastive Learning (GCL) has emerged as a powerful tool for extracting consistent representations from graphs, independent of labeled information. However, existing methods predominantly focus on undirected graphs, disregarding the pivotal directional information that is fundamental and indispensable in real-world networks (e.g., social networks and recommendations). In this paper, we introduce S2-DiGCL, a novel framework that emphasizes spatial insights from complex and real domain perspectives for directed graph (digraph) contrastive learning. From the complex-domain perspective, S2-DiGCL introduces personalized perturbations into the magnetic Laplacian to adaptively modulate edge phases and directional semantics. From the real-domain perspective, it employs a path-based subgraph augmentation strategy to capture fine-grained local asymmetries and topological dependencies. By jointly leveraging these two complementary spatial views, S2-DiGCL constructs high-quality positive and negative samples, leading to more general and robust digraph contrastive learning. Extensive experiments on 7 real-world digraph datasets demonstrate the superiority of our approach, achieving SOTA performance with 4.41% improvement in node classification and 4.34% in link prediction under both supervised and unsupervised settings.

Index Terms—Graph Neural Network, Contrastive Learning, Directed Graph.

I. INTRODUCTION

Graph has become a fundamental data structure for modeling pairwise relationships across diverse domains, such as social interactions [1], [2], transportation networks [3], [4], and recommendation systems [5], [6]. This widespread use has spurred the rapid development of GNNs [7], [8], which effectively capture topological dependencies and node interactions. Despite advancements, conventional supervised GNNs face inherent limitations due to their reliance on extensive labeled data, posing a critical bottleneck as the volume of real-world graphs continues to grow while annotated data remain scarce and expensive to obtain. To mitigate this limitation, GCL [9], [10] has emerged as a promising self-supervised paradigm that learns robust and transferable node representations by enforcing consistency across multiple augmented graph views.

Observation. While current GCL methodologies have demonstrated remarkable success on undirected graphs, their applicability to digraphs remains largely unexplored. The persistent neglect of directional semantics poses a huge challenge to mainstream GCL researches. Owing to the unique advantages and fundamental role of edge directionality in governing information propagation patterns, digraphs motivate us to engage in an in-depth exploration in contrastive learning.

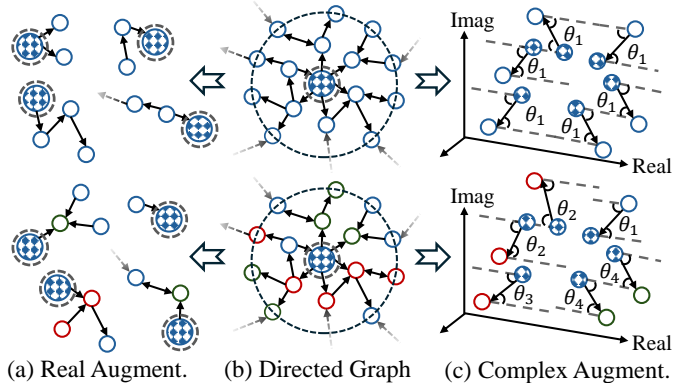


Fig. 1. Illustration of naive (Upper) vs. personalized (Lower) augmentations from real and complex spatial perspectives. Uniform perturbations fail to distinguish heterophilous nodes or asymmetric directional flows, while personalized perturbations adapt augmentation strength and phase shifts to each node's topology, enabling direction-aware contrastive learning in S2-DiGCL.

Motivation. *Digraphs inherently encode directional information flows between entities, providing a more accurate representation of real-world scenarios.* For instance, directional edges in social networks model asymmetric influence propagation among follower-follower relationships [11]; transportation networks require directional edges to simulate one-way traffic constraints and congestion patterns [12]; and citation networks utilize edge directions to represent unidirectional knowledge transfer between scientific publications [13], [14]. Beyond these intuitive examples, recent studies such as A2DUG [15], Dir-GNN [16] and ADPA [17] have revealed a crucial insight: *The direction of edge offers a novel perspective for addressing the challenges of topological heterophily*, a persistent issue in graph learning where connected nodes exhibit dissimilar features. Collectively, these findings highlight the untapped potential of directional information and motivate the development of a dedicated contrastive learning framework for digraphs.

To achieve effective digraph contrastive learning, a straightforward approach is to directly apply augmentation strategies designed for undirected graphs (e.g., random edge dropping or feature masking). However, due to the intrinsic structural asymmetry of directed graphs, such approaches often disrupt directional information flows patterns and consequently yield suboptimal performance. Although several recent investigations into digraph contrastive learning [18], [19] have shown promise, they remain hindered by two notable **Limitations**.

① *Singular Perspective*. Current methods typically restrict their augmentation strategies to either real-valued domain or complex-valued domain. Perturbations in the real domain explicitly capture local directional dependencies, whereas those in the complex domain implicitly encode global rotational semantics via the imaginary components of magnetic Laplacians [20]. However, relying solely on either perspective is insufficient to comprehensively represent the multifaceted characteristics of digraphs. ② *Lack of Personalization*. Current perturbation strategies generally employ uniform augmentation parameters for all nodes, overlooking the inherent diversity in directed topologies and complex semantic contexts unique to each node. For instance, as shown in Fig. 1, hub nodes in citation networks may require different augmentation intensities compared to periphery nodes, owing to their distinct in-degree and out-degree distributions. Such one-size-fits-all strategies hinder the generation of context-aware embeddings by ignoring node-specific characteristics. These limitations reveal an opportunity to advance digraph contrastive learning by designing frameworks that jointly exploit both local and global directional information while incorporating personalized augmentation to adapt to diverse node contexts.

Solution. To address the aforementioned challenges, we propose **S2-DiGCL** (Dual Spatial Directed Graph Contrastive Learning), where ‘S2’ signifies the dual spatial perspectives that jointly model directional information in real and complex domains. S2-DiGCL significantly progresses unsupervised learning on digraphs through two groundbreaking innovations: ① **Comprehensive Perspectives**. We develop a novel path-based augmentation strategy in the real domain to preserve local directional neighborhoods through biased random walks. This approach is complemented by a complex-domain magnetic augmentation mechanism that captures global directional dependencies through the imaginary-space modulation of the magnetic Laplacian. Together, these dual perturbations construct complementary views that encode both local directional interactions and global rotational semantics, enabling a more complete representation of digraph structures. ② **Personalized Augmentation**. We further introduce a personalized magnetic Laplacian augmentation technique, which perturbs both the Laplacian matrix and the digraph structure. This personalization accommodates a diverse range of global-structured patterns and ensures that augmentations align more closely with each node’s unique contextual characteristics. We also enhance the traditional random walk approach by making it adaptive to the unique topology of digraphs, ensuring that the walking process generates personalized perturbations based on the digraph’s specific structural properties. By integrating these dual spatial insights, S2-DiGCL produces high-quality and complementary positive and negative samples, thus enabling more general digraph contrastive learning.

Our contributions. Building upon these core ideas, our work makes the following three key advancements: (1) General Framework. We propose S2-DiGCL, a dual-spatial contrastive learning framework for digraphs that jointly leverages perturbations in both the real and complex domains to maximize the modeling of directional information. (2) Innovative Perturbation Techniques. We devise a path-based

real-domain augmentation to generate local context-level views, complemented by a complex-domain magnetic perturbation that captures global directional dependencies, together enabling a comprehensive representation of digraph structures. (3) SOTA Performance. Extensive experiments on seven real-world digraph datasets demonstrate that S2-DiGCL consistently outperforms strong baselines under both supervised and unsupervised settings, achieving an average improvement of 4.41% in node classification and 4.34% in link prediction.

II. PRELIMINARIES

A. Notation

Let $\mathcal{G} = (\mathcal{V}, \mathcal{E})$ represent a directed graph, where \mathcal{V} and \mathcal{E} represent the sets of nodes and edges, respectively, with $|\mathcal{V}| = n$ and $|\mathcal{E}| = m$. Each node $v \in \mathcal{V}$ is associated with a d -dimensional feature vector, and all node features are stacked into a feature matrix $\mathbf{X} \in \mathbb{R}^{n \times d}$. The topology of directed graph \mathcal{G} is represented by an asymmetrical adjacency matrix $\mathbf{A} = \{0, 1\}^{n \times n}$ that encodes the direction of edges between nodes. Specifically, for any pair of nodes $u, v \in \mathcal{V}$, $\mathbf{A}(u, v) = 1$ if $(u, v) \in \mathcal{E}$, and $\mathbf{A}(u, v) = 0$ vice versa.

B. Graph Contrastive Learning

Graph Contrastive Learning (GCL) has emerged as a paradigm-shifting methodology in self-supervised graph representation learning, effectively addressing the label dependency bottleneck. GCL leverages the intrinsic topological structure of graphs to enforce representation consistency across multiple augmented views without reliance on labels, thereby pulling positive samples closer and pushing negative samples apart in the embedding space. Depending on the granularity of contrastive objectives, existing GCL methods can be categorized into intra-scale and inter-scale approaches.

Intra-scale methods focus on constructing contrastive views at the identical topological granularity. For instance, GraphCL [21] introduces four general graph augmentations (i.e., node dropping, edge perturbation, attribute masking, and subgraph sampling) to learn invariant representations by contrasting differently augmented graph views. It systematically studies how augmentation types and strengths affect performance, revealing that appropriate compositions are crucial for effective representation learning. However, these augmentations require tedious manual tuning and may distort graph semantics. To alleviate this issue, SimGRACE [22] eliminates the need for graph-level augmentations by perturbing the encoder parameters instead of the graph data, achieving comparable or superior performance with higher efficiency and semantic stability.

Inter-scale methods exploit hierarchical information through cross-granularity contrastive objectives, which can be broadly categorized into Global-Local, Global-Context, and Context-Local contrast. DGI [9] is a pioneering work that maximizes mutual information between local node embeddings and the global graph summary, encouraging each node representation to preserve high-level structural semantics. By contrasting real and corrupted graph pairs, DGI effectively bridges node-level and graph-level information,

yielding strong performance on both transductive and inductive tasks. Building upon this, SUBG-CON [23] further enhances scalability and regional awareness by contrasting central nodes with their sampled subgraphs. Instead of relying on the complete graph, SUBG-CON focuses on regional neighborhoods, capturing mid-range dependencies while significantly reducing computational cost and enabling parallelization.

C. Directed Graph Neural Network

Research on directed graph neural networks (DiGNNs) extends traditional undirected GNNs to explicitly model edge directionality. DGCN [24] improves the message aggregation process by integrating multi-order neighborhood proximity, enabling more expressive propagation over directed structures. DiGCN [25] further introduces an α -parameterized steady-state distribution derived from personalized PageRank, formulating a principled approach for directed graph convolution.

Among these advancements, MagNet [20] has emerged as the dominant paradigm that leverages the magnetic Laplacian to perform convolution in the Fourier domain. This formulation encodes the existence of edges in the magnitude of complex entries and their directional information in the phase:

$$\begin{aligned} \mathbf{A}_s(u, v) &= \frac{1}{2} (\mathbf{A}(u, v) + \mathbf{A}(v, u)), \\ \Theta^{(q)}(u, v) &:= 2\pi q (\mathbf{A}(u, v) - \mathbf{A}(v, u)), \\ \mathbf{L}^{(q)} &:= \mathbf{D}_s - \mathbf{A}_s \odot \exp(i\Theta^{(q)}), \end{aligned} \quad (1)$$

where \mathbf{A}_s represents the symmetrized adjacency matrix, \mathbf{D}_s is the corresponding degree matrix, and $\Theta^{(q)}$ denotes the phase matrix controlled by the charge parameter $q \in (0, 0.25]$, which determines the strength of directionality. The real part of $\mathbf{L}^{(q)}$ indicates the edge existence, whereas the imaginary part suggests the asymmetric phases that encode edge directions.

Recently, path-based approaches have gained success in spatial-based GNNs. DiRW [26] introduces a weight-free, direction-aware path sampler that optimizes path generation from the perspectives of walk probability, length, and number by jointly considering node profiles and topological structure.

Despite these advances, most existing DiGNNs still depend heavily on labeled data for supervision. To alleviate this limitation, digraph contrastive learning methods have been proposed to enable unsupervised or self-supervised representation learning. These spatial-based contrastive frameworks operate directly on the digraph structure to integrate message-passing [27], [28] with direction-aware data augmentations. Specifically, DiGCL [18] introduces Laplacian perturbation that perturbs the teleport probability within the approximate directed Laplacian, thereby generating multiple contrastive views without altering the original digraph topology. In contrast, UGCL [19] operates in the complex domain by extending the magnetic Laplacian and perturbing its phase matrix, which explicitly balances the representation of edge existence and directionality. Collectively, these methods demonstrate the potential of contrastive learning in capturing asymmetric structural semantics within directed graphs, yet they still rely on limited or handcrafted perturbations, highlighting the need for more flexible and personalized augmentation strategies.

III. PROPOSED METHOD

In this section, we present S2-DiGCL, a novel contrastive learning framework for digraphs that leverages dual spatial perspectives by jointly modeling perturbations in the real and complex domains. The framework is composed of three main components: (1) A personalized magnetic Laplacian perturbation module that generates node-level representations in the complex domain. (2) A path-based augmentation module that captures context-level subgraph semantics in the real domain. (3) A dual-space contrastive objective that integrates both representations to achieve comprehensive and direction-aware embedding learning. The overall architecture of S2-DiGCL is illustrated in Fig. 2.

A. Complex Domain Personalized Magnetic Perturbation

Recent developments in spectral graph theory have demonstrated that the magnetic Laplacian provides a principled formulation for representing digraphs. Building on this foundation, several studies [19], [20], [29] have utilized the magnetic Laplacian to encode edge directionality by introducing a complex-valued phase matrix parameterized by a charge value q . In contrast to the conventional graph Laplacian, which assumes bidirectional edges, the magnetic Laplacian naturally models asymmetric dependencies through complex phases, making it particularly suitable for analyzing the structural and spectral properties of digraphs.

The central innovation of S2-DiGCL lies in its *personalized magnetic perturbation mechanism*, which adaptively modulates the magnetic potential field of each directed edge through a topology-aware phase coefficient. By introducing edge-specific variations of the charge parameter q , this mechanism dynamically alters the phase of the magnetic Laplacian, enabling node-dependent propagation that reflects both local structural uncertainty and global directional asymmetry. This design enriches the model's capacity to capture diverse and complex directional patterns across different regions of the digraph. Inspired by MAP [30], we first measure the *topological uncertainty* of each node v by quantifying the balance between its in-degree and out-degree distributions:

$$U_v = - \left(\frac{\tilde{d}_v^{\text{in}}}{m} \log \frac{\tilde{d}_v^{\text{in}}}{m} + \frac{\tilde{d}_v^{\text{out}}}{m} \log \frac{\tilde{d}_v^{\text{out}}}{m} \right) / \log 2, \quad (2)$$

where m is the number of edges in the digraph. A higher value of U_v indicates a more balanced in-out structure, implying greater directional ambiguity. For each directed edge (u, v) , we define a *topological modulation coefficient* and obtain the *personalized charge* as:

$$q_{uv}^* = q_0 \cdot q_{uv}^{\text{topo}}, \quad q_{uv}^{\text{topo}} = \tanh \left(\frac{U_u + U_v}{\text{mean}(U)} \right), \quad (3)$$

which emphasizes edges connecting nodes with high directional uncertainty. Here $q_0 \in (0, 0.25]$ is a global base charge controlling the overall phase magnitude. This formulation provides a parameter-free yet edge-specific adaptation of the magnetic potential, ensuring that structurally ambiguous regions receive stronger directional perturbations.

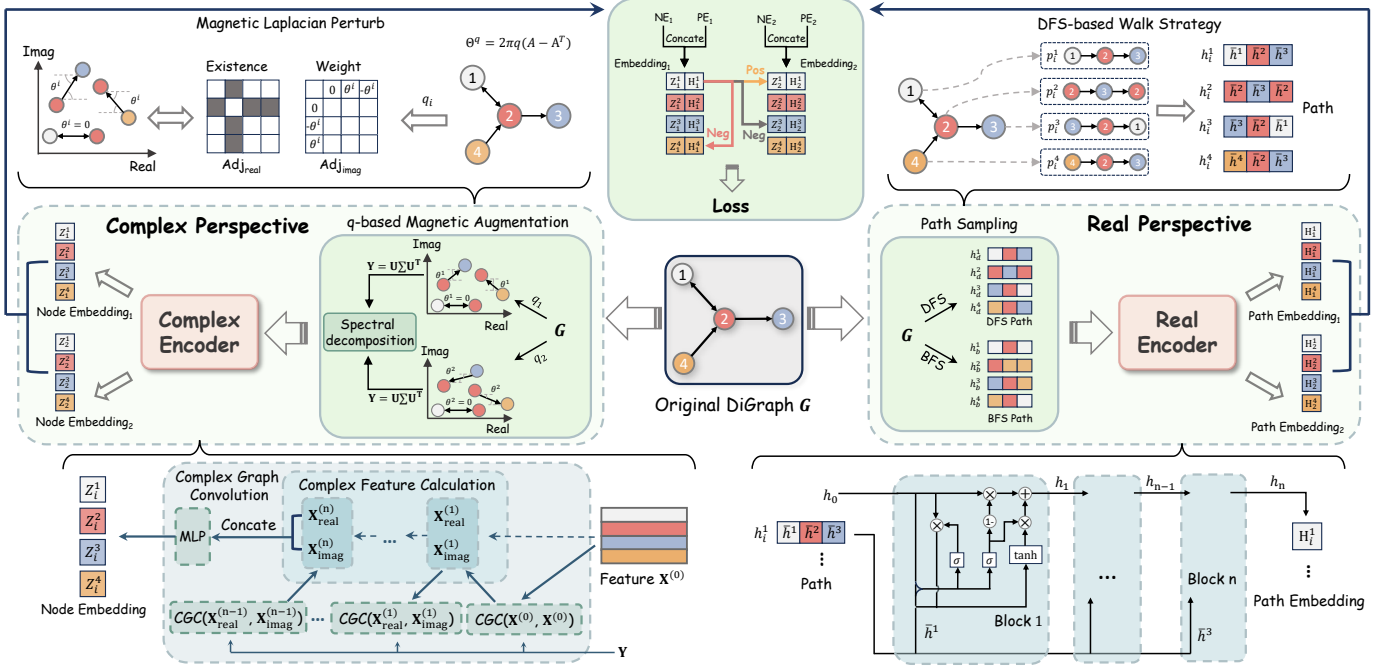


Fig. 2. Overview of S2-DiGCL, including a complex-domain global personalized magnetic Laplacian augmentation (Left), a real-domain local path augmentation (Right) and a novel contrastive strategy that combines both perspectives (Upper).

To incorporate stochastic directional variability, we further introduce a *probabilistic perturbation factor* defined as:

$$\Phi_r^{(q^*)}(u, v) = \begin{cases} q_{uv}^*, & \text{with probability } r, \\ 1 - q_{uv}^*, & \text{with probability } 1 - r, \end{cases} \quad (4)$$

where $r \in [0, 1]$ controls the likelihood of maintaining the original edge orientation. A larger r favors the original directionality, while a smaller r introduces greater structural perturbation. This stochastic mechanism implicitly reverses edge directions in a probabilistic manner, introducing diversity without explicit graph rewiring. The resulting phase matrix integrates both directionality and uncertainty:

$$\Theta_r^{(q^*)}(u, v) = 2\pi (\mathbf{A}(u, v) - \mathbf{A}(v, u)) \odot \Phi_r^{(q^*)}(u, v), \quad (5)$$

where \odot denotes the element-wise product. Notably, it is easy to see that $\Theta^{(q^*)}(u, v) = -\Theta^{(1-q^*)}(v, u)$ from Eq. (1), meaning that simply perturbing q^* is equivalent to topologically reversing edge directions in a probabilistic manner. The random perturbation in $\Phi_r^{(q^*)}$ actually corresponds to a random perturbation of the direction of the directed edges, reflecting the concept of personalized perturbation without explicit edge redirecting. Beyond topological perturbations, we further introduce a Laplacian augmentation, where q^* is perturbed by a small term Δq . This yields the **personalized magnetic Laplacian perturbation**:

$$\mathbf{L}_{r, \Delta q}^{(q^*)} := \mathbf{D}_s - \mathbf{A}_s \odot \exp(i\Theta_r^{(q^* + \Delta q)}), \quad (6)$$

where Δq is a perturbation term that satisfies $q^* + \Delta q \in [0, 0.25]$ to avoid excessive phase shifts. Through this operation, the sparsity of the magnetic Laplacian matrix is maintained, which means it can be directly used to the subsequent GNN-based encoders.

With the personalized magnetic Laplacian in place, we follow the standard GCL protocol based on paired spectral views. Specifically, S2-DiGCL constructs two correlated Laplacian views, the original $\mathbf{L}^{(q^*)}$ and the perturbed $\mathbf{L}_{r, \Delta q}^{(q^*)}$. These views are fed into a shared complex-valued graph convolutional encoder, where each layer updates both the real and imaginary parts of node features.

Taking $\mathbf{L}^{(q^*)}$ as an example, the l -th layer is written as:

$$\begin{aligned} \mathbf{X}_{\text{real}}^{(l)} &= \left(\mathbf{D}_s^{-\frac{1}{2}} \mathbf{A}_s \mathbf{D}_s^{-\frac{1}{2}} \odot \exp(i\Theta^{(q^*)}) \right) \mathbf{X}_{\text{real}}^{(l-1)}, \\ \mathbf{X}_{\text{imag}}^{(l)} &= \left(\mathbf{D}_s^{-\frac{1}{2}} \mathbf{A}_s \mathbf{D}_s^{-\frac{1}{2}} \odot \exp(i\Theta^{(q^*)}) \right) \mathbf{X}_{\text{imag}}^{(l-1)}, \end{aligned} \quad (7)$$

with $\mathbf{X}_{\text{real}}^{(0)} = \mathbf{X}_{\text{imag}}^{(0)} = \mathbf{X}^{(0)}$ denoting the initial node features.

After stacking L convolutional layers, we flatten the complex output by concatenating the two parts and obtain the final node embeddings via an MLP:

$$\text{NE} = \text{MLP} \left(\mathbf{X}_{\text{real}}^{(L)} \parallel \mathbf{X}_{\text{imag}}^{(L)} \right), \quad (8)$$

where \parallel denotes concatenation. The same encoder is applied to the perturbed view $\mathbf{L}_{r, \Delta q}^{(q^*)}$, yielding a correlated pair of complex-domain representations for contrastive learning.

B. Real Domain Path Augmentation

While the complex-domain magnetic Laplacian perturbation captures global directional patterns through phase shifts, the local flow of information within digraphs is equally important for tasks that require fine-grained structural awareness. Recent work [26] has shown that walk-based approaches are particularly effective at encoding such local directionality by explicitly modeling node sequences along directed paths.

To complement the global complex-domain representation, we propose a path augmentation framework that generates subgraph-level views in the real domain. For each node, we employ both Breadth-First Search (BFS) and Depth-First Search (DFS) strategies to sample two distinct directed walk sequences. Guided by the homophily principle [31], BFS-generated sequences capture local structure patterns that are homophilous with the central node, whereas DFS-generated sequences explore longer-range heterophilous neighbors.

To control the path sampling behavior, we introduce a second-order direction-aware sampler characterized by two parameters p and q , which govern the trade-off between local and global exploration, similar to Node2Vec [32]. Consider a random walk that has just traversed the edge (u, v) and currently resides at node v . For all outgoing edges (v, x) , the unnormalized transition probability α is defined as:

$$\alpha(v, x) = \begin{cases} 1/p, & \text{if } d_{ux} = 0, \\ 1, & \text{if } d_{ux} = 1, \\ 1/q, & \text{if } d_{ux} = 2, \\ 0, & \text{otherwise,} \end{cases} \quad (9)$$

where d_{ux} denotes the shortest-path distance between u and x . Setting $0 < p < 1$ and $q > 1$ biases the walk toward BFS-like local exploration, whereas $p > 1$ and $0 < q < 1$ promote DFS-like deeper traversal. For each node v_i in the digraph, we generate two sequences h_b^i and h_d^i based on BFS and DFS:

$$\begin{aligned} \mathbf{P}_b &= \{h_b^1, h_b^2, \dots, h_b^n\}, \\ \mathbf{P}_d &= \{h_d^1, h_d^2, \dots, h_d^n\}, \end{aligned} \quad (10)$$

where h_b^i denotes the BFS-based path sequence sampled with node v_i as the central node. Similarly, h_d^i represents the DFS-based path sequence derived from the node v_i .

Given a path list \mathbf{P} , the path aggregator f_{path} plays a crucial role in transforming the raw path sequences into comprehensive path embeddings (PE). These embeddings are designed to effectively capture the intricate local topology surrounding the central node, thereby providing a rich representation of the node's neighborhood. Crucially, the aggregator must preserve both the node order and directionality of the sequences to maintain structural fidelity. We implement f_{path} as a gated recurrent unit (GRU) [33], a variant of RNNs with gating mechanisms that mitigate vanishing gradients in long sequences, particularly effective for capturing the sequential relationships among the nodes within the path. It processes each sequence stepwise, updating a hidden state that encapsulates the path's directional context up to the current node. For a sequence $h^i = \{v_1^i, v_2^i, \dots, v_l^i\}$, the GRU computes:

$$\begin{aligned} \mathbf{z}^t &= \sigma(\mathbf{W}_z [\mathbf{h}^{t-1}, \mathbf{x}^t]), \\ \mathbf{r}^t &= \sigma(\mathbf{W}_r [\mathbf{h}^{t-1}, \mathbf{x}^t]), \\ \hat{\mathbf{h}}^t &= \tanh(\mathbf{W}_h [\mathbf{r}^t \odot \mathbf{h}^{t-1}, \mathbf{x}^t]), \\ \mathbf{h}^t &= (1 - \mathbf{z}^t) \odot \mathbf{h}^{t-1} + \mathbf{z}^t \odot \hat{\mathbf{h}}^t, \end{aligned} \quad (11)$$

where \mathbf{z}^t and \mathbf{r}^t are update and reset gates, respectively, and \mathbf{h}^t is the hidden state at step t . The final embedding for the sequence is derived from the last hidden state \mathbf{h}^l , which encodes the cumulative directional flow of the entire path.

C. Contrastive Objective

To unify the global and local representations, we fuse the embeddings obtained from the two spatial perspectives. Specifically, the node embeddings \mathbf{NE}_1 and \mathbf{NE}_2 are produced from the complex-domain personalized magnetic Laplacian perturbation, while the path embeddings \mathbf{PE}_1 and \mathbf{PE}_2 are generated from the real-domain path augmentation. The final representations are formed by concatenating the two types of embeddings and passing them through a projection head:

$$\begin{aligned} \mathbf{E}_1 &= g(\mathbf{NE}_1 \parallel \mathbf{PE}_1), \\ \mathbf{E}_2 &= g(\mathbf{NE}_2 \parallel \mathbf{PE}_2), \end{aligned} \quad (12)$$

where $g(\cdot)$ denotes a nonlinear projection that maps the fused embeddings into a shared latent space suitable for contrastive learning. The goal of the contrastive objective is to maximize agreement between two correlated views of the same node while distinguishing them from other nodes. Let \mathbf{h}_i^1 and \mathbf{h}_i^2 denote the embeddings of the i -th node in \mathbf{E}_1 and \mathbf{E}_2 , respectively. The pair $(\mathbf{h}_i^1, \mathbf{h}_i^2)$ is treated as a positive sample, and all other combinations are treated as negatives. In this way, the model is encouraged to produce view-invariant representations that capture consistent semantics across both spatial domains. To quantify this alignment, we employ the InfoNCE [34] objective, which estimates a lower bound of the mutual information (MI) between the two embedding distributions. The total loss consists of two components:

$$\begin{aligned} \mathcal{L}_{\text{inter}} &= -\frac{1}{n} \sum_{i=1}^n \log \frac{\exp(\mathcal{S}(\mathbf{h}_i^1, \mathbf{h}_i^2) / \tau)}{\sum_{j=1}^n \exp(\mathcal{S}(\mathbf{h}_i^1, \mathbf{h}_j^2) / \tau)}, \\ \mathcal{L}_{\text{intra}} &= -\frac{1}{2n} \sum_{k=1}^2 \sum_{i=1}^n \log \frac{1}{\sum_{j \neq i} \exp(\mathcal{S}(\mathbf{h}_i^k, \mathbf{h}_j^k) / \tau)}, \\ \mathcal{L} &= \mathcal{L}_{\text{inter}} + \mathcal{L}_{\text{intra}}, \end{aligned} \quad (13)$$

where $\mathcal{S}(\cdot, \cdot)$ denotes cosine similarity and τ is a temperature coefficient controlling the concentration of the similarity distribution.

Here, $\mathcal{L}_{\text{inter}}$ enforces consistency between the complex-domain and real-domain views by pulling positive pairs closer across modalities, while $\mathcal{L}_{\text{intra}}$ maintains local smoothness within each view by discouraging over-collapsed representations. Jointly optimizing these two terms enables S2-DiGCL to balance semantic alignment and structural diversity, ensuring that the learned embeddings are simultaneously discriminative and direction-aware across both spatial domains.

IV. THEORETICAL ANALYSIS

A. Magnetic Von Neumann Entropy

The magnetic Laplacian introduces a complex-valued perturbation to the spectral domain of a directed graph through the charge parameter q , which modulates the relative strength between edge existence and direction. To quantitatively assess the structural impact of this perturbation, we employ the concept of *Von Neumann entropy* [35], originally designed to measure the spectral complexity of graphs, and extend it to the magnetic Laplacian setting.

Definition 1 (Magnetic Von Neumann Entropy): Let $\mathcal{G} = (\mathcal{V}, \mathcal{E})$ be a directed graph with $n = |\mathcal{V}|$ nodes and a magnetic Laplacian $\mathbf{L}^{(q)}$. We define the normalized density matrix as

$$\rho^{(q)} = \frac{\exp(-\beta\mathbf{L}^{(q)})}{\text{Tr}[\exp(-\beta\mathbf{L}^{(q)})]}, \quad (14)$$

where $\beta > 0$ is a scaling temperature parameter controlling spectral smoothness. The *magnetic Von Neumann entropy* of \mathcal{G} is then defined as:

$$H_{VN}(\mathcal{G}, q) = -\text{Tr}[\rho^{(q)} \log \rho^{(q)}]. \quad (15)$$

This definition generalizes the classical Von Neumann entropy to the complex domain. When $q = 0$, the magnetic Laplacian $\mathbf{L}^{(q)}$ reduces to the symmetric Laplacian of the undirected version of \mathcal{G} , thereby recovering the standard graph entropy $H_{VN}(\mathcal{G})$. As q increases, the imaginary component of $\mathbf{L}^{(q)}$ perturbs the spectral distribution, effectively redistributing the eigenvalue magnitudes and thus altering the entropy. In this sense, $H_{VN}(\mathcal{G}, q)$ captures the degree of structural uncertainty arising from directional asymmetry.

Definition 2 (Perturbation Entropy Variation): Given a small charge perturbation Δq in the charge parameter, we define the *entropy variation* as:

$$\Delta H_{VN}(\mathcal{G}, q, \Delta q) = H_{VN}(\mathcal{G}, q + \Delta q) - H_{VN}(\mathcal{G}, q). \quad (16)$$

A positive ΔH_{VN} indicates that the spectrum becomes uniform (i.e., high uncertainty), while a negative value suggests increasing concentration of eigenenergy on a few modes.

Intuitively, ΔH_{VN} quantifies how sensitive the spectral structure of a digraph is to directional perturbations introduced by the magnetic potential. This entropy-based measure forms the foundation for our subsequent theoretical analysis, where we establish its spectral properties and interpret the physical implications of such perturbations in directed graph learning.

B. Spectral Properties of Magnetic Perturbation

The magnetic Laplacian $\mathbf{L}^{(q)}$ is a Hermitian matrix for $q \in [0, 1/2]$, hence it admits an eigen-decomposition $\mathbf{L}^{(q)} = \mathbf{U}^{(q)} \text{diag}(\lambda^{(q)}) \mathbf{U}^{(q)*}$ with real eigenvalues $\{\lambda_k^{(q)}\}_{k=1}^n$. Define the Gibbs-Boltzmann spectral weights

$$p_k^{(q)} = \frac{e^{-\beta\lambda_k^{(q)}}}{Z^{(q)}}, \quad Z^{(q)} = \sum_{j=1}^n e^{-\beta\lambda_j^{(q)}}, \quad (17)$$

so that

$$\begin{aligned} H_{VN}(\mathcal{G}, q) &= -\sum_{k=1}^n p_k^{(q)} \log p_k^{(q)} \\ &= \beta \mathbb{E}_{p^{(q)}}[\lambda^{(q)}] + \log Z^{(q)}. \end{aligned} \quad (18)$$

Theorem 1 (Monotonic Entropy Response): Assume that $\mathbf{L}^{(q)}$ depends smoothly on q and that eigenvalues are simple almost everywhere (so that $\lambda_k^{(q)}$ are differentiable a.e.). Then

$$\frac{\partial H_{VN}}{\partial q} = -\beta^2 \text{Cov}_{p^{(q)}}(\lambda^{(q)}, \dot{\lambda}^{(q)}), \quad \dot{\lambda}_k^{(q)} = \frac{\partial \lambda_k^{(q)}}{\partial q}. \quad (19)$$

Consequently, the sign of $\partial H_{VN}/\partial q$ is governed by the correlation between eigenvalues and their q -sensitivities: if higher-frequency modes (i.e., larger $\lambda_k^{(q)}$) grow faster in q than lower ones, then H_{VN} decreases (i.e., the spectrum sharpens); otherwise H_{VN} increases (i.e., the spectrum flattens).

Proof. Using $H_{VN} = \beta \mathbb{E}_{p^{(q)}}[\lambda] + \log Z$, we have

$$\frac{\partial H_{VN}}{\partial q} = \beta \frac{\partial}{\partial q} \mathbb{E}_{p^{(q)}}[\lambda] + \frac{\partial}{\partial q} \log Z^{(q)}. \quad (20)$$

By standard differentiation under the Gibbs measure,

$$\frac{\partial}{\partial q} \mathbb{E}_{p^{(q)}}[\lambda] = \mathbb{E}_{p^{(q)}}[\dot{\lambda}] - \beta \text{Cov}_{p^{(q)}}(\lambda, \dot{\lambda}), \quad (21)$$

and

$$\begin{aligned} \frac{\partial}{\partial q} \log Z^{(q)} &= \frac{1}{Z^{(q)}} \sum_k e^{-\beta\lambda_k^{(q)}} (-\beta \dot{\lambda}_k^{(q)}) \\ &= -\beta \mathbb{E}_{p^{(q)}}[\dot{\lambda}]. \end{aligned} \quad (22)$$

Combining the two identities cancels the $\mathbb{E}_{p^{(q)}}[\dot{\lambda}]$ terms and yields $\frac{\partial H_{VN}}{\partial q} = -\beta^2 \text{Cov}_{p^{(q)}}(\lambda, \dot{\lambda})$. \square

To bound finite changes in entropy, we next relate the centered variability of $\dot{\lambda}^{(q)}$ to matrix perturbations of $\mathbf{L}^{(q)}$.

Theorem 2 (Bounded Entropy Variation): For any finite Δq , let $\Delta \mathbf{L} = \mathbf{L}^{(q+\Delta q)} - \mathbf{L}^{(q)}$. Then there exists $\xi \in (q, q + \Delta q)$ such that:

$$|\Delta H_{VN}(\mathcal{G}, q, \Delta q)| \leq \frac{\beta^2}{\sqrt{n}} \sigma_{\lambda}^{(\xi)} \|\Delta \mathbf{L}\|_F, \quad (23)$$

where $\sigma_{\lambda}^{(\xi)}$ is the standard deviation (under $p^{(\xi)}$) of $\{\lambda_k^{(\xi)}\}_{k=1}^n$. Therefore, magnetic perturbations induce bounded entropy change, ensuring controlled spectral diversity.

Proof. By the mean-value theorem applied to $q \mapsto H_{VN}(\mathcal{G}, q)$, there exists $\xi \in (q, q + \Delta q)$ with

$$\begin{aligned} \Delta H_{VN} &= \frac{\partial H_{VN}}{\partial q} \Big|_{q=\xi} \Delta q \\ &= -\beta^2 \text{Cov}_{p^{(\xi)}}(\lambda^{(\xi)}, \dot{\lambda}^{(\xi)}) \Delta q. \end{aligned} \quad (24)$$

Taking absolute values and Cauchy-Schwarz for covariance,

$$|\Delta H_{VN}| \leq \beta^2 \sigma_{\lambda}^{(\xi)} \sigma_{\dot{\lambda}}^{(\xi)} |\Delta q|, \quad (25)$$

where $\sigma_{\dot{\lambda}}^{(\xi)}$ is the standard deviation of $\{\dot{\lambda}_k^{(\xi)}\}$ under $p^{(\xi)}$. Now relate $\sigma_{\dot{\lambda}}^{(\xi)}$ to matrix perturbations. Write $\Delta \lambda = \lambda^{(q+\Delta q)} - \lambda^{(q)} \in \mathbb{R}^n$. By the Hoffman-Wielandt inequality for Hermitian matrices,

$$\|\Delta \lambda\|_2 \leq \|\Delta \mathbf{L}\|_F. \quad (26)$$

By a mean-value argument on each $\lambda_k(q)$, there exists the same ξ such that $\Delta \lambda = \dot{\lambda}^{(\xi)} \Delta q$, hence $\|\dot{\lambda}^{(\xi)}\|_2 |\Delta q| \leq \|\Delta \mathbf{L}\|_F$. Since the standard deviation is bounded by the ℓ_2 norm scaled by $1/\sqrt{n}$,

$$\sigma_{\dot{\lambda}}^{(\xi)} \leq \frac{1}{\sqrt{n}} \|\dot{\lambda}^{(\xi)}\|_2 \leq \frac{1}{\sqrt{n}} \frac{\|\Delta \mathbf{L}\|_F}{|\Delta q|}. \quad (27)$$

Substituting into the covariance bound gives $|\Delta H_{VN}| \leq \beta^2 \sigma_{\lambda}^{(\xi)} \frac{1}{\sqrt{n}} \|\Delta \mathbf{L}\|_F$, as claimed. \square

TABLE I
STATISTICS OF THE DATASETS USED IN EXPERIMENTS.

Dataset	#Nodes	#Edges	#Features	#Classes	Train/Valid/Test	Description
CoraML	2,995	8,416	2,879	7	140/500/2355	Citation network
Citeseer	3,312	4,591	3,703	6	120/500/2692	Citation network
Pubmed	19,717	88,648	500	3	60/500/19157	Citation network
Actor	7,600	26,659	932	5	3648/2432/1520	Co-occurrence network
WikiCS	11,701	290,519	300	10	580/1769/5847	Weblink network
Chameleon	890	13,534	2,325	5	409/287/194	Weblink network
Squirrel	2,223	65,578	2,089	5	1053/718/452	Weblink network

C. Interpretation and Implications

The preceding results establish that magnetic perturbations in the complex domain have two desirable theoretical properties that directly explain the effectiveness of our method.

a) Controlled Structural Diversity: The monotonic entropy response in Theorem 1 indicates that the Von Neumann entropy $H_{VN}(\mathcal{G}, q)$ changes smoothly with the charge parameter q . When q increases, the entropy either rises or falls monotonically depending on how the eigenvalues respond to the perturbation. This ensures that varying q systematically adjusts the structural complexity of the digraph, enabling the generation of multiple views with gradually increasing or decreasing spectral diversity. Such controllable diversity is crucial for contrastive learning, which benefits from correlated yet non-identical views.

b) Stability of Magnetic Perturbation: The bounded variation in Theorem 2 guarantees that the entropy change caused by finite perturbations is limited by Eq. (23). This implies that the magnetic augmentation introduces diversity without destabilizing the spectrum. In practice, the personalized perturbations Δq_i in S2-DiGCL remain within this stable range, ensuring that node-level augmentations preserve the overall topology while enriching directional semantics.

c) Implications for Contrastive Learning: Together, these two properties justify the design of the complex-domain branch in S2-DiGCL. Monotonicity ensures that each perturbed view reflects a consistent structural shift, while boundedness guarantees spectral smoothness across views. Consequently, the model can produce informative yet coherent contrastive pairs, which are diverse enough to enhance representation learning, but stable enough to maintain semantic alignment. This theoretical foundation explains why the magnetic perturbation yields effective and robust digraph contrastive learning in our framework.

V. EXPERIMENTS

In this section, we present a comprehensive empirical evaluation of S2-DiGCL to validate its effectiveness across multiple downstream tasks and diverse real-world digraph datasets. Our experiments are systematically designed to address the following four key research questions: **Q1 (Model Performance):** Does S2-DiGCL achieve superior performance compared to existing unsupervised and supervised baselines? **Q2 (Component Contributions):** How do the real-domain path augmentation and complex-domain magnetic perturbation

modules individually and jointly contribute to the model's performance? **Q3 (Robustness):** How robust is S2-DiGCL to variations in key hyperparameters? **Q4 (Computational Efficiency):** How efficient is S2-DiGCL in terms of training time and convergence speed?

A. Experimental Setup

1) Datasets: To comprehensively evaluate the proposed framework, we conduct experiments on seven widely used real-world directed graph datasets, covering three distinct network typologies: citation networks, co-occurrence networks, and weblink networks. These datasets collectively cover a broad spectrum of structural characteristics, including varying graph scales, feature dimensionalities, and degrees of homophily and heterophily. Table I summarizes their key statistics, and detailed descriptions are provided below.

Citation networks (CoraML, Citeseer, Pubmed). Each node in these datasets corresponds to a scientific publication, and each directed edge represents a citation link from one paper to another [36], [37]. These graphs are widely used to benchmark graph representation learning methods due to their clear directional semantics, relatively balanced topology, and strong community structures driven by academic subfields. **CoraML** consists of machine learning papers represented by bag-of-words features. It serves as a canonical benchmark for semi-supervised classification on homophilous graphs, where connected papers often discuss similar research topics and exhibit dense intra-class citation links. **Citeseer** focuses on computer science publications across multiple subdomains, featuring higher sparsity and stronger class imbalance than CoraML. The dataset's weakly homophilous structure and fragmented communities make it a more challenging scenario for learning consistent embeddings across heterogeneous citation patterns. **Pubmed** contains biomedical research papers represented by TF-IDF weighted word vectors. With nearly twenty thousand nodes and dense citation relationships, it provides a information-rich benchmark for evaluating both scalability and representation robustness in directed settings.

Co-occurrence network (Actor). The **Actor** dataset [38] is constructed from the IMDb platform, where nodes represent actors and directed edges indicate co-appearances in films. Unlike citation networks, the Actor graph exhibits pronounced structural heterophily, as actors connected by an edge often belong to different genres or professional circles. This property results in complex local neighborhoods with diverse attribute

distributions, making the dataset particularly suitable for evaluating the ability of digraph models to capture cross-domain and non-homophilous relationships.

Weblink networks (WikiCS, Chameleon, Squirrel). In these datasets, each node corresponds to a web page and each directed edge denotes a hyperlink between pages [39], [40]. Such graphs are inherently asymmetric and densely connected, providing a realistic setting for analyzing information propagation and hierarchical dependencies in digraphs. **WikiCS** forms a large-scale network of computer science concepts extracted from English Wikipedia, characterized by high average node degree and rich semantic interconnections between topics, an ideal benchmark for studying large, dense digraphs with high topic overlap. **Chameleon** focuses on region-specific Wikipedia pages with clear community boundaries and moderate graph density, enabling detailed analysis of local structural consistency and community-level information flow. **Squirrel**, on the other hand, centers on environmental science topics and exhibits irregular connectivity patterns with multi-scale dependencies and noisy hyperlinks. These properties make it a challenging benchmark for testing model robustness and generalization under complex, heterogeneous digraph topologies.

2) *Baselines*: We compare S2-DiGCL with a broad range of baseline methods covering both supervised and unsupervised paradigms, as well as undirected and directed graph settings. To ensure a fair and comprehensive evaluation, we group these baselines into four categories according to their learning paradigm and graph type. The technical characteristics of each category are summarized as follows.

(i) *Supervised undirected GNNs*. **GCN** [41] is a spectral-based GNN that approximates the graph Laplacian via first-order Chebyshev polynomials, enabling efficient neighborhood aggregation and structural encoding. **GAT** [42] introduces masked self-attention mechanisms to assign adaptive weights to neighboring nodes, allowing each node to selectively attend to informative neighbors. **RAW-GNN** [43] integrates random walk strategies into message passing by combining breadth-first walks for homophilous information and depth-first walks for heterophilous information, thereby improving generalization across different graph homophily levels.

(ii) *Supervised directed GNNs*. **DiGCN** [25] extends spectral graph convolution to directed graphs by leveraging personalized PageRank to capture directional dependencies and learn multi-resolution structural features. **MagNet** [20] models directionality in digraphs through a complex-valued spectral formulation based on the magnetic Laplacian, where edge phases encode orientation information via complex eigenvectors.

(iii) *Unsupervised undirected GCLs*. **DGI** [9] maximizes mutual information between local node embeddings and a global summary vector, encouraging representations that preserve global graph semantics. **GCA** [44] performs adaptive graph augmentations guided by topological importance, effectively emphasizing critical structural patterns during contrastive learning. **GraphCL** [45] employs a variety of graph augmentations (e.g., node dropping, edge perturbation) to generate distinct yet semantically consistent graph views for contrastive training. **GRACE** [10] constructs multiple contrastive views through both structural and attribute perturba-

tions, aligning corresponding node embeddings across these views to achieve invariant representations.

(iv) *Unsupervised directed GCLs*. **DiGCL** [18] generates phase-shifted views via edge direction-aware perturbations within the spectral domain, explicitly incorporating directional semantics while preserving digraph connectivity. **UGCL** [19] unifies the magnetic Laplacian with contrastive learning by introducing complex-valued perturbation matrices that capture both edge existence and orientation, providing a generalized framework for digraph contrastive learning.

3) *Implementation Details*: Our implementation strategy is adapted to the characteristics of each downstream task. For the link prediction task, we follow the widely adopted data-split convention from prior studies [20], [46], where 80% of the edges are used for training, 15% for validation, and the remaining 5% for testing. For all unsupervised methods, including our proposed S2-DiGCL, label information is utilized only during the evaluation stage. Specifically, we employ the standard linear evaluation protocol [9]. In this protocol, the encoder is first trained in a fully unsupervised manner using the contrastive objective to learn node representations without label supervision. Once pre-training is completed, the encoder parameters are frozen, and a logistic regression classifier is trained on the learned node embeddings using the training labels. The classifier is then evaluated on the test set to assess the quality of the learned representations independently from the influence of the downstream model. This evaluation scheme ensures a fair comparison across different methods and isolates the representation learning ability of each model from classifier capacity. To ensure experimental reliability, all reported results are averaged over five independent runs with different random seeds. We present the mean performance together with the corresponding standard deviation, providing a consistent view of each model's robustness and stability.

4) *Experimental Environment*: All experiments are conducted on a high-performance computing node equipped with an Intel(R) Xeon(R) Platinum 8468V CPU and an NVIDIA H800 PCIe GPU, running CUDA 12.2. The operating system is Ubuntu 20.04.6 LTS, and the software stack consists of Python 3.8 and PyTorch 2.2.1. All baseline implementations are based on their official repositories or open-source reimplementations, and hyperparameters are tuned to ensure reproducibility and fairness across all experimental settings.

B. Overall Performance

To address **Q1**, we conduct extensive experiments comparing S2-DiGCL with all baseline methods across three representative tasks: node classification, link prediction, and t-SNE-based cluster visualization. These tasks jointly evaluate the discriminative power, structural awareness, and embedding interpretability of the learned node representations.

1) *Node Classification Performance*: To assess the quality and generalizability of the learned node embeddings, we perform node classification experiments on all benchmark datasets. The results are summarized in Table II.

We observe that conventional unsupervised baselines (e.g., DGI, GRACE), which are primarily designed for undirected

TABLE II
NODE CLASSIFICATION PERFORMANCE. THE BEST RESULT IS **BOLD**. THE SECOND RESULT IS UNDERLINED.

Method	CoraML	Citeseer	WikiCS	Actor	Pubmed	Chameleon	Squirrel	
SUPERVISED	GCN	<u>80.90±0.36</u>	<u>65.57±0.60</u>	77.56±0.29	31.20±0.51	78.19±0.17	43.20±1.80	37.74±1.08
	GAT	80.17±1.09	63.76±1.71	77.00±0.83	29.41±1.25	79.83±0.30	41.44±4.04	34.20±1.24
	RAW-GNN	76.51±0.87	59.38±0.81	75.09±0.26	<u>35.08±0.53</u>	76.45±0.31	42.78±0.96	38.45±2.92
	DiGCN	77.94±0.35	62.24±0.50	77.63±0.46	33.91±1.02	76.60±0.20	40.52±3.43	37.65±1.14
	MagNet	79.41±1.05	63.91±1.27	76.74±0.70	31.26±0.67	77.34±0.63	43.09±2.77	40.97±1.11
UNSUPERVISED	DGI	72.55±2.29	57.30±4.07	74.19±2.90	30.67±0.63	74.32±1.87	39.95±1.76	34.73±1.24
	GCA	80.39±1.11	65.30±1.38	72.82±1.90	29.39±0.97	<u>71.05±4.04</u>	39.38±0.86	41.72±1.13
	GraphCL	74.93±1.68	62.65±1.71	<u>78.37±0.77</u>	31.51±1.54	73.20±1.82	43.59±1.38	39.29±3.60
	GRACE	78.34±0.84	63.49±1.33	70.49±3.13	30.72±0.63	74.15±2.42	41.84±2.08	40.75±1.01
	UGCL	78.66±1.52	64.20±1.70	75.43±3.15	33.63±0.70	76.15±4.02	<u>44.49±1.43</u>	39.99±1.57
S2-DiGCL	DiGCL	77.83±2.57	63.36±2.23	74.83±2.88	34.53±0.42	79.14±1.16	<u>42.66±1.21</u>	38.50±0.68
	S2-DiGCL	81.83±1.37	67.68±0.63	78.42±1.13	35.71±0.84	79.16±0.81	45.18±2.42	41.95±1.46

TABLE III
LINK PREDICTION PERFORMANCE. THE BEST RESULT IS **BOLD**. THE SECOND RESULT IS UNDERLINED.

	Existence				Direction				
	CoraML	Citeseer	Chameleon	Squirrel	CoraML	Citeseer	Chameleon	Squirrel	
SUPERVISED	GCN	75.81±0.58	<u>69.87±0.60</u>	84.05±0.42	87.24±0.10	84.01±0.26	82.46±2.12	87.50±0.53	87.22±0.17
	GAT	72.27±1.50	<u>67.16±1.55</u>	83.17±1.89	85.88±1.96	82.56±2.53	<u>79.91±2.09</u>	87.18±2.70	86.98±1.96
	RAW-GNN	77.69±0.60	69.04±0.96	<u>84.47±0.58</u>	88.43±0.16	<u>89.72±1.21</u>	86.79±1.25	<u>90.43±1.20</u>	88.95±0.15
	DiGCN	78.90±0.16	67.21±0.36	83.82±0.39	88.28±0.14	88.20±0.38	86.29±1.52	90.21±0.69	84.91±0.10
	MagNet	79.38±0.67	69.48±1.19	83.73±0.25	<u>88.47±0.12</u>	89.57±0.42	86.07±1.43	90.32±0.58	86.90±0.28
UNSUPERVISED	DGI	72.12±0.98	63.65±1.98	80.30±1.02	84.66±2.97	85.71±1.36	77.59±1.51	84.10±4.03	83.77±2.57
	GCA	75.93±1.06	64.32±0.77	82.69±0.64	86.63±0.26	80.87±0.94	76.79±1.64	82.34±1.20	83.45±0.32
	GraphCL	75.74±0.89	66.29±2.26	82.12±0.81	83.06±1.81	88.37±0.54	77.05±2.91	89.47±1.04	<u>89.17±0.31</u>
	GRACE	74.31±0.63	65.76±1.12	81.91±0.82	86.57±0.21	80.03±0.74	85.68±2.56	83.24±2.29	83.01±0.77
	UGCL	73.64±1.09	66.55±2.01	79.47±0.98	83.93±1.36	85.52±1.68	79.51±1.04	87.44±1.87	84.60±4.91
S2-DiGCL	DiGCL	76.48±1.59	64.72±2.32	81.66±0.94	85.23±0.24	83.32±3.39	76.88±1.61	86.65±0.85	82.48±1.11
	S2-DiGCL	79.60±1.45	71.57±1.25	87.57±0.89	89.46±0.40	89.80±0.75	86.37±1.69	91.04±2.13	89.76±1.54

graphs, exhibit substantial performance degradation on directed datasets. This performance drop can be attributed to their inherent assumption of bidirectional message passing and their inability to explicitly model asymmetric edge relationships. In contrast, direction-aware contrastive methods such as DiGCL and UGCL achieve notable improvements by incorporating spectral or complex-domain perturbations that respect edge directionality. However, their augmentation strategies are limited to a single representation space, either real or complex, which constrains their ability to capture multi-domain relational semantics. Our proposed S2-DiGCL bridges this gap by jointly modeling real-domain path augmentations and complex-domain magnetic perturbations, effectively integrating structural and directional cues in a complementary manner. This dual-domain learning scheme consistently achieves the highest accuracy across all datasets. Despite being entirely unsupervised, S2-DiGCL attains comparable or even superior performance to several supervised GNNs, including RAW-GNN and MagNet. It ranks first on six out of seven benchmarks and secures the second-best result on WikiCS, demonstrating that S2-DiGCL can capture task-relevant structure without relying on labeled data. Beyond classification

accuracy, S2-DiGCL also exhibits remarkable stability. Across five independent runs, the variance of its performance remains consistently lower than that of competing methods, particularly on datasets characterized by noisy or sparse connections (e.g., Citeseer and Squirrel). This robustness indicates that S2-DiGCL learns more invariant and topology-aware representations, maintaining reliability under diverse graph conditions.

2) *Link Prediction Performance*: To further examine the generality of our framework, we conduct link prediction experiments on four representative datasets: CoraML, Citeseer, Chameleon, and Squirrel. This task evaluates whether the learned representations can effectively capture both topological connectivity and directional dependencies between nodes. We adopt two evaluation settings: *Existence*, which predicts whether an edge exists between two nodes, and *Direction*, which determines the orientation of an existing edge.

As summarized in Table III, our proposed S2-DiGCL consistently outperforms both supervised and unsupervised baselines in the Existence setting, demonstrating the efficacy of the dual-spatial augmentation strategy in learning coherent node embeddings that generalize across missing or perturbed connections. In the more challenging Direction set-

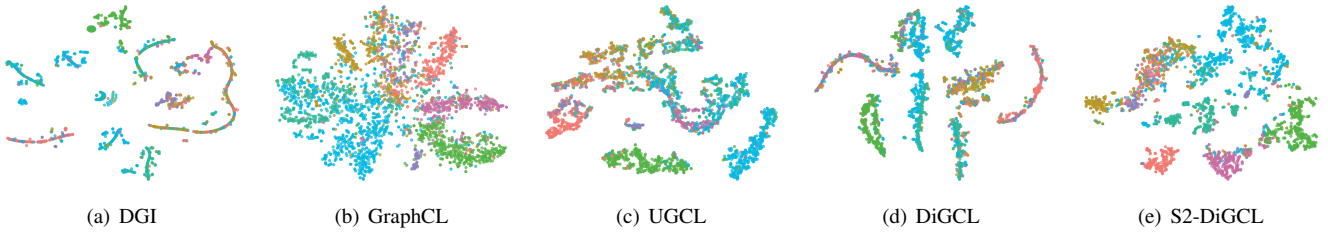


Fig. 3. Visualization results on CoraML.

TABLE IV
ABLATION STUDY ON CORA ML AND CITESEER.

Variant	CoraML		CiteSeer	
	Node	Link	Node	Link
w/o complex	71.41 \pm 1.48	82.29 \pm 2.10	62.68 \pm 1.49	76.54 \pm 3.41
w/o real	73.18 \pm 1.92	85.51 \pm 1.70	64.84 \pm 1.48	82.56 \pm 2.46
w/o perturb	69.81 \pm 2.12	84.21 \pm 2.15	61.17 \pm 0.57	79.29 \pm 1.42
uniform perturb	70.68 \pm 2.98	82.48 \pm 1.57	61.98 \pm 1.47	80.46 \pm 2.87
w/o direction	71.50 \pm 1.87	83.47 \pm 1.23	62.04 \pm 0.74	76.76 \pm 2.45
w/o RNN	70.42 \pm 1.44	84.09 \pm 0.80	61.18 \pm 2.69	78.07 \pm 1.21
S2-DiGCL	81.83\pm1.37	89.80\pm0.75	67.68\pm0.63	86.37\pm1.69

ting, unsupervised methods tailored for digraphs (e.g., UGCL, DiGCL) exhibit superior performance over their undirected counterparts (e.g., DGI, GCA, GraphCL, GRACE), confirming the importance of explicitly modeling edge asymmetry in digraphs. Building upon these approaches, S2-DiGCL further enhances directional prediction accuracy by jointly integrating real-domain path augmentations with complex-domain magnetic perturbations. This dual-domain formulation allows the model to simultaneously capture global connectivity cues and fine-grained directional dependencies. These results highlight that S2-DiGCL not only learns discriminative node embeddings without label supervision but also generalizes effectively across two link prediction scenarios.

3) *Visualization*: To intuitively demonstrate the representation quality of S2-DiGCL compared with other unsupervised baselines, we visualize the learned node embeddings from the CoraML using t-SNE [47]. The results are shown in Fig. 3, where different colors correspond to different node classes.

The embeddings produced by GraphCL appear widely scattered, with blurred class boundaries and significant overlap between clusters. By comparison, DGI, UGCL, and DiGCL yield more compact and coherent clusters, indicating that these models better capture local structural patterns. Nevertheless, both DGI and UGCL still display partially overlapping regions, suggesting that the learned representations are not fully discriminative in the latent space. In contrast, S2-DiGCL produces clearly separated and compact clusters, where nodes of the same class are closely grouped while different classes occupy distinct regions in the embedding space. This observation indicates that the dual spatial learning mechanism effectively enhances the semantic separability of node representations. The qualitative patterns observed here are consistent with the quantitative improvements reported in node classification and link prediction, further confirming the representational effectiveness of S2-DiGCL.

C. Ablation Study

To address **Q2**, we perform an ablation study on the CoraML and CiteSeer datasets to examine the contribution of each component within S2-DiGCL. The analysis focuses on three key aspects: augmentation perspectives, personalized perturbations, and path augmentation. Table IV reports the results for both node classification (Node) and link direction prediction (Link).

1) *Augmentation Perspectives*: We begin by disabling either the real-domain or complex-domain perturbation to analyze their individual effects. The results show that removing either component leads to a noticeable drop in accuracy across both tasks, confirming that the two spatial perspectives contribute complementary information. In particular, removing the complex-domain augmentation results in a more pronounced performance decline compared with removing the real-domain component. This observation suggests that the personalized magnetic Laplacian perturbation in the complex domain not only captures directional semantics but also models higher-order structural dependencies that are critical for digraph representation learning.

2) *Personalized Perturbations*: Next, we evaluate the role of the personalized magnetic Laplacian perturbation by comparing two simplified variants. The *w/o perturb* and *uniform perturb* settings correspond to fixing the personalization coefficient r in Eq. (4) to 0.0 and 1.0, respectively. Both variants lead to a significant reduction in performance, indicating that the adaptive perturbation mechanism is essential for capturing diverse local contexts. The results confirm that allowing node-specific perturbation strengths enables the model to better preserve structural nuances, especially in graphs exhibiting high heterogeneity or varying local connectivity.

3) *Path Augmentation*: Finally, we investigate the effect of the path sampler and the design of the real-domain encoder. In the *w/o direction* variant, the model ignores edge direction during path sampling, which weakens its ability to model asymmetric neighborhood structures. This limitation particularly affects the understanding of directional relationships between central nodes and their neighbors. Similarly, replacing the RNN-based encoder with an MLP in the *w/o RNN* variant removes the sequential modeling capability required to encode ordered path information. Both variants exhibit notable performance degradation compared with the complete S2-DiGCL model. These findings highlight that directionality and sequence modeling play indispensable roles in capturing hierarchical and sequential dependencies within digraphs.

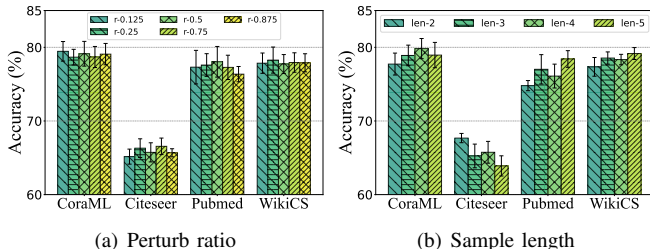


Fig. 4. Performance with different parameters.

D. Sensitivity Analysis

To address **Q3**, we perform sensitivity experiments to examine the influence of key hyperparameters on the performance of S2-DiGCL in the node classification task. The analysis is conducted on four representative datasets: CoraML, Citeseer, Pubmed, and WikiCS. We focus on two critical parameters that directly affect the dual-domain learning process: ① the perturbation ratio r within the personalized magnetic Laplacian, and ② the path length l within the direction-aware path sampler. The corresponding results are illustrated in Fig. 4.

1) *Perturbation Ratio*: We vary the perturbation ratio r across the range [0.125, 0.25, 0.5, 0.75, 0.875] to assess how the intensity of magnetic perturbation influences representation learning. As shown in Fig. 4(a), the performance of S2-DiGCL remains consistently stable across all datasets, with only minor fluctuations. This observation suggests that the personalized magnetic Laplacian perturbation effectively balances structural smoothness and local adaptability, enabling the model to capture both global and local topological information. The robustness to variations in r further indicates that S2-DiGCL does not rely on fine-tuned parameter settings, which enhances its practicality across diverse digraph scenarios.

2) *Path Length*: We also analyze the impact of the path length l in the direction-aware path sampler by varying it among [2, 3, 4, 5]. The trends depicted in Fig. 4(b) show that the optimal value of l differs across datasets, with CoraML achieving its peak performance at $l = 4$, Citeseer at $l = 2$, and both Pubmed and WikiCS at $l = 5$. These results reveal a trade-off between capturing sufficient directional information and avoiding noise propagation. Shorter paths may fail to model higher-order directional dependencies, leading to incomplete neighborhood representations, while excessively long paths may accumulate redundant or noisy information, particularly in sparse graphs such as Citeseer. Overall, the consistent performance across a moderate range of l values demonstrates that S2-DiGCL achieves a good balance between expressiveness and stability in modeling digraph structures.

E. Efficiency Analysis

To address **Q4**, we evaluate the computational efficiency of S2-DiGCL with respect to convergence speed and total training time, comparing it against all unsupervised baselines on Citeseer. The experimental results are presented in Fig. 5.

1) *Convergence Speed*: To evaluate convergence behavior, we monitor the classification accuracy of each model over training time. As shown in Fig. 5(a), S2-DiGCL converges within approximately 15 seconds while maintaining a steadily

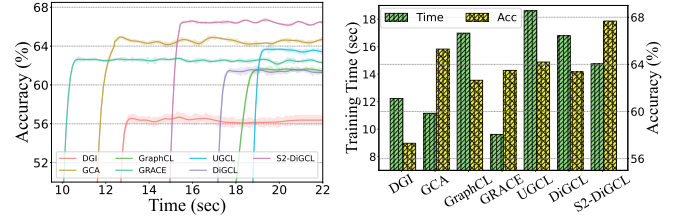


Fig. 5. Time efficiency on Citeseer.

increasing accuracy throughout the training process. This convergence pattern indicates that the dual spatial learning strategy facilitates more efficient optimization by promoting rapid alignment between the real and complex representation spaces. Although methods such as DGI, GCA, and GRACE reach convergence slightly earlier, their final accuracies are notably lower. These results suggest that S2-DiGCL achieves a balance between convergence speed and representation quality, enabling efficient yet effective learning on digraphs.

2) *Training Time*: We further compare the total training time and final accuracy of all models, as summarized in Fig. 5(b). S2-DiGCL achieves the highest accuracy among all unsupervised methods while maintaining competitive training time. This outcome demonstrates that the proposed dual-domain design does not introduce substantial computational overhead despite its additional modeling capacity. The efficient optimization behavior can be attributed to the complementary nature of the real-domain path augmentation and the complex-domain magnetic perturbation, which together enable faster convergence and more stable gradient propagation. Overall, these results confirm that S2-DiGCL attains both high accuracy and strong computational efficiency, making it well suited for large-scale directed graph learning.

VI. CONCLUSION

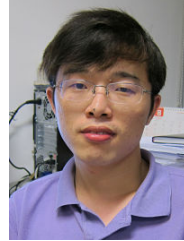
In this paper, we introduced S2-DiGCL, a novel framework for contrastive learning on digraphs that unifies the strengths of complex- and real-domain representations. The proposed dual spatial perspective effectively addresses the challenge of modeling inherent directionality in GCL. By incorporating personalized perturbations within the magnetic Laplacian, S2-DiGCL captures global directional dependencies, while its path-based subgraph augmentation strategy preserves local asymmetric information flows. Extensive experiments on seven real-world datasets verify that S2-DiGCL consistently outperforms SOTA supervised and unsupervised approaches on both node- and link-level tasks. These results highlight the framework's strong capability in learning robust, direction-aware graph representations without label supervision. Beyond its empirical performance, the dual-domain design of S2-DiGCL offers a generalizable perspective for extending contrastive learning to other forms of structured data, such as temporal networks and knowledge graphs, where directional semantics are fundamental to information propagation. Although the current augmentation process introduces additional computational cost on large-scale graphs, future work will focus on developing more efficient sampling and perturbation mechanisms to further enhance scalability and practicality.

REFERENCES

- [1] A. Mislove, M. Marcon, K. P. Gummadi, P. Druschel, and B. Bhattacharjee, "Measurement and analysis of online social networks," in *Proceedings of the 7th ACM SIGCOMM conference on Internet measurement*, 2007, pp. 29–42.
- [2] R. Kumar, J. Novak, and A. Tomkins, "Structure and evolution of online social networks," in *Proceedings of the 12th ACM SIGKDD international conference on Knowledge discovery and data mining*, 2006, pp. 611–617.
- [3] J. Lin and Y. Ban, "Complex network topology of transportation systems," *Transport reviews*, vol. 33, no. 6, pp. 658–685, 2013.
- [4] A. Háznyag, I. Fi, A. London, and T. Nemeth, "Complex network analysis of public transportation networks: A comprehensive study," in *2015 International Conference on Models and Technologies for Intelligent Transportation Systems (MT-ITS)*. IEEE, 2015, pp. 371–378.
- [5] S. Wu, F. Sun, W. Zhang, X. Xie, and B. Cui, "Graph neural networks in recommender systems: a survey," *ACM Computing Surveys*, vol. 55, no. 5, pp. 1–37, 2022.
- [6] D. Su, B. Fan, Z. Zhang, H. Fu, and Z. Qin, "Dcl: Diversified graph recommendation with contrastive learning," *IEEE Transactions on Computational Social Systems*, 2024.
- [7] P. Reiser, M. Neubert, A. Eberhard, L. Torresi, C. Zhou, C. Shao, H. Metni, C. van Hoesel, H. Schopmans, T. Sommer *et al.*, "Graph neural networks for materials science and chemistry," *Communications Materials*, vol. 3, no. 1, p. 93, 2022.
- [8] Z. Wu, S. Pan, F. Chen, G. Long, C. Zhang, and S. Y. Philip, "A comprehensive survey on graph neural networks," *IEEE Transactions on Neural Networks and Learning Systems*, vol. 32, no. 1, pp. 4–24, 2020.
- [9] P. Veličković, W. Fedus, W. L. Hamilton, P. Liò, Y. Bengio, and R. D. Hjelm, "Deep Graph Infomax," in *International Conference on Learning Representations, ICLR*, 2019.
- [10] Y. Zhu, Y. Xu, F. Yu, Q. Liu, S. Wu, and L. Wang, "Deep graph contrastive representation learning," *arXiv preprint arXiv:2006.04131*, 2020.
- [11] M. Gupte, P. Shankar, J. Li, S. Muthukrishnan, and L. Iftode, "Finding hierarchy in directed online social networks," in *Proceedings of the 20th international conference on World wide web*, 2011, pp. 557–566.
- [12] S. Marshall, J. Gil, K. Kropf, M. Tomko, and L. Figueiredo, "Street network studies: from networks to models and their representations," *Networks and Spatial Economics*, vol. 18, pp. 735–749, 2018.
- [13] N. P. Hummon and P. Dereian, "Connectivity in a citation network: The development of dna theory," *Social networks*, vol. 11, no. 1, pp. 39–63, 1989.
- [14] S. A. Greenberg, "How citation distortions create unfounded authority: analysis of a citation network," *Bmj*, vol. 339, 2009.
- [15] S. Maekawa, Y. Sasaki, and M. Onizuka, "Why using either aggregated features or adjacency lists in directed or undirected graph? empirical study and simple classification method," *arXiv preprint arXiv:2306.08274*, 2023.
- [16] E. Rossi, B. Charpentier, F. D. Giovanni, F. Frasca, S. Günnemann, and M. Bronstein, "Edge directionality improves learning on heterophilic graphs," in *Proceedings of The European Conference on Machine Learning and Principles and Practice of Knowledge Discovery in Databases, ECML-PKDD Workshop*, 2023.
- [17] H. Sun, X. Li, Z. Wu, D. Su, R.-H. Li, and G. Wang, "Breaking the entanglement of homophily and heterophily in semi-supervised node classification," *arXiv preprint arXiv:2312.04111*, 2023.
- [18] Z. Tong, Y. Liang, H. Ding, Y. Dai, X. Li, and C. Wang, "Directed graph contrastive learning," *Advances in neural information processing systems*, vol. 34, pp. 19 580–19 593, 2021.
- [19] T. Ko, Y. Choi, and C.-K. Kim, "Universal graph contrastive learning with a novel laplacian perturbation," in *Uncertainty in Artificial Intelligence*. PMLR, 2023, pp. 1098–1108.
- [20] X. Zhang, Y. He, N. Brugnone, M. Perlmutter, and M. Hirn, "Magnet: A neural network for directed graphs," *Advances in Neural Information Processing Systems, NeurIPS*, 2021.
- [21] Y. You, T. Chen, Y. Sui, T. Chen, Z. Wang, and Y. Shen, "Graph contrastive learning with augmentations," *Advances in neural information processing systems*, vol. 33, pp. 5812–5823, 2020.
- [22] J. Xia, L. Wu, J. Chen, B. Hu, and S. Z. Li, "Simgrace: A simple framework for graph contrastive learning without data augmentation," in *Proceedings of the ACM Web Conference 2022*, 2022, pp. 1070–1079.
- [23] Y. Jiao, Y. Xiong, J. Zhang, Y. Zhang, T. Zhang, and Y. Zhu, "Sub-graph contrast for scalable self-supervised graph representation learning," in *2020 IEEE international conference on data mining (ICDM)*. IEEE, 2020, pp. 222–231.
- [24] Z. Tong, Y. Liang, C. Sun, D. S. Rosenblum, and A. Lim, "Directed graph convolutional network," *arXiv preprint arXiv:2004.13970*, 2020.
- [25] Z. Tong, Y. Liang, C. Sun, X. Li, D. Rosenblum, and A. Lim, "Digraph inception convolutional networks," *Advances in Neural Information Processing Systems, NeurIPS*, 2020.
- [26] D. Su, X. Li, Z. Li, Y. Liao, R.-H. Li, and G. Wang, "Dirw: Path-aware digraph learning for heterophily," *arXiv preprint arXiv:2410.10320*, 2024.
- [27] K. Xu, C. Li, Y. Tian, T. Sonobe, K.-i. Kawarabayashi, and S. Jegelka, "Representation learning on graphs with jumping knowledge networks," in *International Conference on Machine Learning, ICML*, 2018.
- [28] W. Zhang, Z. Yin, Z. Sheng, Y. Li, W. Ouyang, X. Li, Y. Tao, Z. Yang, and B. Cui, "Graph attention multi-layer perceptron," *Proceedings of the ACM SIGKDD Conference on Knowledge Discovery and Data Mining, KDD*, 2022.
- [29] S. Furutani, T. Shibahara, M. Akiyama, K. Hato, and M. Aida, "Graph signal processing for directed graphs based on the hermitian laplacian," in *Joint European Conference on Machine Learning and Knowledge Discovery in Databases, ECML-PKDD*. Springer, 2020.
- [30] X. Li, D. Su, Z. Wu, G. Zeng, H. Qin, R.-H. Li, and G. Wang, "Toward effective digraph representation learning: A magnetic adaptive propagation based approach," in *Proceedings of the ACM on Web Conference 2025*, 2025, pp. 2908–2923.
- [31] M. McPherson, L. Smith-Lovin, and J. M. Cook, "Birds of a feather: Homophily in social networks," *Annual Review of SocioLoGy*, vol. 27, no. 1, pp. 415–444, 2001.
- [32] A. Grover and J. Leskovec, "Node2vec: Scalable feature learning for networks," in *Proceedings of the ACM SIGKDD Conference on Knowledge Discovery and Data Mining, KDD*, 2016.
- [33] K. Cho, B. Van Merriënboer, C. Gulcehre, D. Bahdanau, F. Bougares, H. Schwenk, and Y. Bengio, "Learning phrase representations using rnn encoder-decoder for statistical machine translation," *arXiv preprint arXiv:1406.1078*, 2014.
- [34] A. v. d. Oord, Y. Li, and O. Vinyals, "Representation learning with contrastive predictive coding," *arXiv preprint arXiv:1807.03748*, 2018.
- [35] C. Ye, R. C. Wilson, C. H. Comin, L. d. F. Costa, and E. R. Hancock, "Approximate von neumann entropy for directed graphs," *Physical Review E*, vol. 89, no. 5, p. 052804, 2014.
- [36] A. Bojchevski and S. Günnemann, "Deep gaussian embedding of graphs: Unsupervised inductive learning via ranking," in *ICLR Workshop on Representation Learning on Graphs and Manifolds*, 2018.
- [37] Z. Yang, W. W. Cohen, and R. Salakhutdinov, "Revisiting semi-supervised learning with graph embeddings," in *International Conference on Machine Learning, ICML*, 2016.
- [38] H. Pei, B. Wei, K. C.-C. Chang, Y. Lei, and B. Yang, "Geom-gcn: Geometric graph convolutional networks," in *International Conference on Learning Representations, ICLR*, 2020.
- [39] P. Mernyei and C. Cangea, "Wiki-cs: A wikipedia-based benchmark for graph neural networks," *arXiv preprint arXiv:2007.02901*, 2020.
- [40] B. Rozemberczki, C. Allen, and R. Sarkar, "Multi-Scale attributed node embedding," *Journal of Complex Networks*, vol. 9, no. 2, 05 2021.
- [41] T. N. Kipf and M. Welling, "Semi-supervised classification with graph convolutional networks," in *International Conference on Learning Representations, ICLR*, 2017.
- [42] P. Veličković, G. Cucurull, A. Casanova, A. Romero, P. Lio, and Y. Bengio, "Graph attention networks," in *International Conference on Learning Representations, ICLR*, 2018.
- [43] D. Jin, R. Wang, M. Ge, D. He, X. Li, W. Lin, and W. Zhang, "Raw-gnn: Random walk aggregation based graph neural network," in *Proceedings of the International Joint Conference on Artificial Intelligence, IJCAI*, 2022.
- [44] Y. Zhu, Y. Xu, F. Yu, Q. Liu, S. Wu, and L. Wang, "Graph contrastive learning with adaptive augmentation," in *Proceedings of the web conference 2021*, 2021, pp. 2069–2080.
- [45] H. Hafidi, M. Ghogho, P. Ciblat, and A. Swami, "Negative sampling strategies for contrastive self-supervised learning of graph representations," *Signal Processing*, vol. 190, p. 108310, 2022.
- [46] X. Li, M. Liao, Z. Wu, D. Su, W. Zhang, R.-H. Li, and G. Wang, "Lightdic: A simple yet effective approach for large-scale digraph representation learning," *arXiv preprint arXiv:2401.11772*, 2024.
- [47] L. Van der Maaten and G. Hinton, "Visualizing data using t-sne," *Journal of machine learning research*, vol. 9, no. 11, 2008.



Daohan Su is currently working toward the master's degree in the School of Computer Science & Technology, Beijing Institute of Technology. He received his bachelor's degree from the same institution in 2024. His research interests lie in the areas of graph neural networks and large language models.



Rong-Hua Li received his PhD degree from the Department of Systems Engineering and Engineering Management, The Chinese University of Hong Kong in 2013 and joined the School of Computer and Software, Shenzhen University this year. He joined the School of Computer Science & Technology, Beijing Institute of Technology in 2018 as a professor. His research interests include graph theory, graph computing system, spectral graph theory, graph neural networks and knowledge graph. He is the committee member of VLDB 2024, KDD 2023, WWW 2023.



Yang Zhang received his Bachelor's degree in Computer Science and Technology from Beijing Institute of Technology in 2024, and his Master's degree in Information Engineering from The Chinese University of Hong Kong in 2025. His research interests focus on graph neural networks.



Guoren Wang received his MS, BS and PhD degrees from Northeastern University in 1988, 1991 and 1996. He joined the School of Computer Science & Technology, Beijing Institute of Technology in 2018 as a professor. He is the member of the Discipline Evaluation Group of the State Council and the Expert Review Group of the Information Science Department of the National Natural Science Foundation of China. His research interests include uncertain data management, data intensive computing, visual media data analysis, and bioinformatics.



Xunkai Li is currently working toward the PhD degree with the school of Computer Science & Technology, Beijing Institute of Technology, advised by Prof. Rong-Hua Li. He received the BS degree in computer science from Shandong University in 2022. His research interest lies in general Data-centric ML and Graph-ML in complex scenarios (directed, signed, hypergraph, and distributed). He has published 5+ papers in top DB/DM/AI conferences such as VLDB, WWW, AAAI.